plotted in Fig. 3 the radial field components at the input and output to the horn just discussed. For low frequencies (see Fig. 3*a*), given the relatively low permittivity of the core material in the throat region of the horn, the excitation at the input is approximately that of the fandamental TE_{11} mode for the same-sized circular waveguide. At the output, however, we obtain good symmetry between the radial electric and magnetic fields, indicating an appropriate choice of gap thickness for hybrid-mode operation. For higher frequencies (Fig. 3*b*), the excitation at the input more closely resembles that of a pure HE_{11} mode. With negligible field at the metallic walls of the feed, we can see that the guiding structure is now essentially the dielectric. The hybrid mode is effectively launched at the foam termination, and is basically unaffected by the remaining length of the feed. This feature is maintained up to 30GHz and beyond. In the vicinity of 6 – 7GHz, there is some degree of overlap between the two mechanisms involved, providing a smooth transition between the two modes of operation. Thus good pattern symmetry and low cross-polar can be maintained continuously over an extremely large bandwidth.

Multi-frequency band applications: The characteristics of our cone-loaded feed makes it attractive for use in dual-band applications. A scaled version of the cone-loaded feed of Fig. 1 has been used in an application where two 24% bandwidths were required over a 3:1 frequency separation. The band splitting was achieved by a dielectrically loaded coaxial diplexing junction where the inner conductor of the coaxial waveguide accommodates a dielectrically loaded circular waveguide to support the high-frequency band, while the low-frequency band (cut off at the small circular waveguide size) passes through the coaxial section. The measured results were in excellent agreement with the predictions and this horn is now in service on an earth-station antenna (Details of the design and results of this feed/diplexer system are currently being prepared for publication [4]).

Conclusion: We have described a dielectrically loaded hybrid-mode feed that can operate continuously over an extremely large bandwidth with bandwidth ratios > 30:1. Two mechanisms are responsible for the hybrid-mode operation, where their overlap provides for the extremely wide continuous bandwidth. The challenge now is to use this type of horn fully with effective means of diplexing multiple-frequency bands at the input to the horn.

31 July 1995
Electronics Letters Online No: 19951364

P.R. Clark and G.L. James (*CSIRO Division of Radiophysics, PO Box 76, Epping, NSW 2121, Australia*)

References

1 JAMES, G.L.: 'Design of wide-band compact corrugated horns', *IEEE Trans.*, 1984, **Ap-32**, (10), pp. 1134–1138
2 CLARRICOATS, P.J.B., OLVER, A.D., and RIZK, M.S.A.S.: 'A dielectric loaded conical feed with cross-polar radiation'. Proc. URSI Symp. Electromag. Theory, Santiago, Spain, 1983, pp. 351–354
3 LIER, E.: 'A dielectric hybrid mode antenna feed: A simple alternative to the corrugated horn', *IEEE Trans.*, 1986, **AP-34**, (1), pp. 21–29
4 JAMES, G.L., and CLARK, P.R.: 'A hybrid mode horn with diplexer for dual wideband applications'. In preparation.

In vivo measurement of frequency characteristics of phase velocity of bone with bending vibration

H. Kanai, M. Park and N. Chubachi

Indexing terms: Biomedical engineering, Doppler measurement

The authors propose a new method of measuring the frequency characteristics of phase velocity along a bone for bending vibration modes to diagnose its mechanical characteristics. By introducing a simple model of a distributed-constant network, the phase velocity is determined for each frequency from the spatial distribution of velocity along a radius bone surface which is measured by the ultrasonic Doppler method.

Introduction: In the literature, there have been acoustical approaches for *in vivo* evaluation of bone quality for noninvasive diagnosis of osteoporosis using vibrations of low frequency of less than several kilohertz [1]. The propagation velocity of the longitudinal elastic wave, c_b, which is the square root of the ratio of the Young's modulus to the average density, ρ, is evaluated by measuring the resonant frequency f_0 of a bone when the bone is excited by forced vibration. In these approaches, acceleration pick-ups on the skin surface are employed to measure the bone vibration. Due to the characteristics of the vibration propagating in the flesh between the skin and the bone, the measurable points are limited.

In our previous paper [2], it was demonstrated that the spatial distribution of the velocity on the surface of a bone with forced vibration of low frequency can be directly measured using standard ultrasonic Doppler diagnosis equipment. The obtained velocity distribution is investigated to fit well to the distributed-constant-network model to determine the wavelength $\lambda_b(f_0)$, from which phase velocity $c_b(f_0)$ of the bending-vibration of a bone is determined for one of the resonant frequencies, f_0.

In this letter we propose a new method of measuring the frequency characteristics of phase velocity $c_b(f)$ and the propagation velocity of the longitudinal wave, c_l, is determined from the gradient of the frequency characteristics of $c_b(f)$, which is proportional to $f^{1/2}$. The principle of velocity measurement, simulation experiments with a metal beam, and *in vivo* experiments with a human radius bone are described.

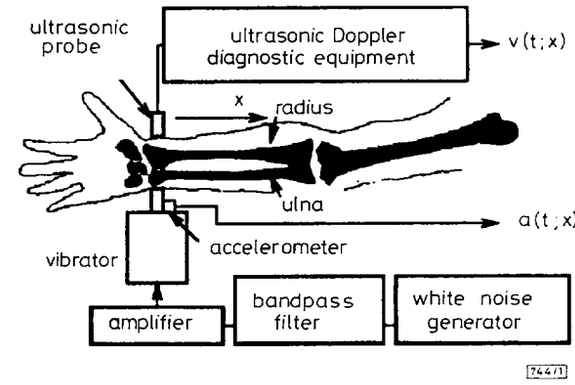

Fig. 1 *Block diagram of in vivo measurement of forced bending vibration of surface of radius using ultrasonic Doppler diagnosis equipment*

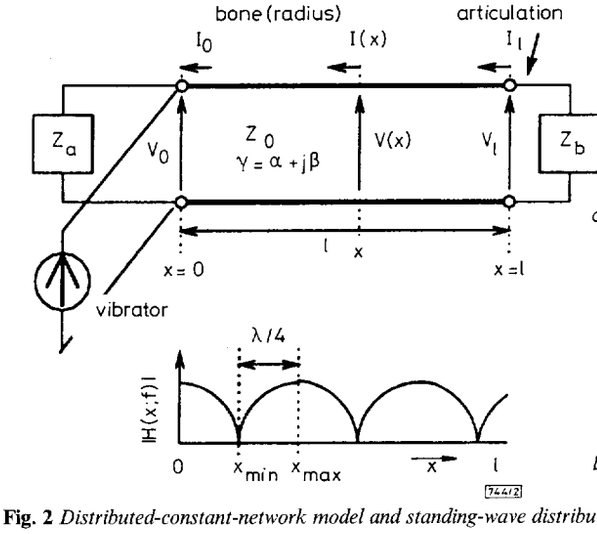

Fig. 2 *Distributed-constant-network model and standing-wave distribution*

a Radius of bone is approximated by a uniform beam, and bending vibration of bone surface is described by distributed-constant-network model
b Wavelength is determined from distribution of a standing wave

Principle: Fig. 1 illustrates measurement of the spatial distribution of the velocity component $v(t; x)$, which is perpendicular to the bone axis on the surface of the radius due to the bending vibration when standard ultrasonic Doppler diagnosis equipment is used. Let us assume that the radius in Fig. 1 is expressed by a uniform beam with length l and a mechanical characteristic impedance Z_0,

and that both ends are terminated by mechanical impedances Z_a and Z_b. Thus, the bending vibration in the bone is described by a distributed-constant-network model in Fig. 2*a*. At the point $x = 0$, where the distal ulna is in contact with the distal radius, bending vibration is induced by a large-scale actuator. Since the actuator employed is of large scale, it is described by a constant current source having infinite internal impedance. Let us describe the force and the vibration velocity $v(t; x)$ of the bending vibration at point x by voltage $V(x)$ and current $I(x)$, respectively, in Fig. 2*a* as follows:

$$V(x) = Z_0 I_0^+ \exp(\gamma x) + Z_0 I_0^- \exp(-\gamma x)$$
$$I(x) = I_0^+ \exp(\gamma x) - I_0^- \exp(-\gamma x) \quad (1)$$

where I_0^+ and I_0^- are the currents of the incident and reflected waves at $x = 0$, respectively, and γ is the propagation constant. To compensate the phase of the driving signal, the transfer function $H(f; x)$, from the output signal $a(t; x)$ of the acceleration pick-up on the actuator head to $v(t; x)$, is introduced by

$$H(f;x) = \frac{\mathrm{E}[A^*(f;x) \cdot B(f;x)]}{\mathrm{E}[|A(f;x)|^2]} \quad (2)$$

where E[·] and * are the average operation and complex conjugate, respectively, and $A(f; x)$ and $B(f; x)$ are the Fourier spectra of $a(t; x)$ and $v(f; x)$, respectively. From the distance between the maximum point x_{max} and the local minimum point x_{min} around x_{max} on the spatial distribution $|H(f; x)|$ in Fig. 2*b*, the wavelength $\lambda_b(f)$ of the standing wave on the surface of the bone is determined by $\lambda_b(f) = 4|x_{max} - x_{min}|$. Thus, the phase velocity $c_b(f)$ is obtained by $c_b(f) = \lambda_b(f) \cdot f$. On the other hand, it is theoretically well known that $c_b(f)$ is given by

$$c_b(f) = \sqrt{\pi r c_l f} \quad (3)$$

where r and c_l are the radius of the columnar beam and the velocity of the longitudinal wave, respectively. Thus, from the frequency characteristics of $c_b(f)$, c_l is determined.

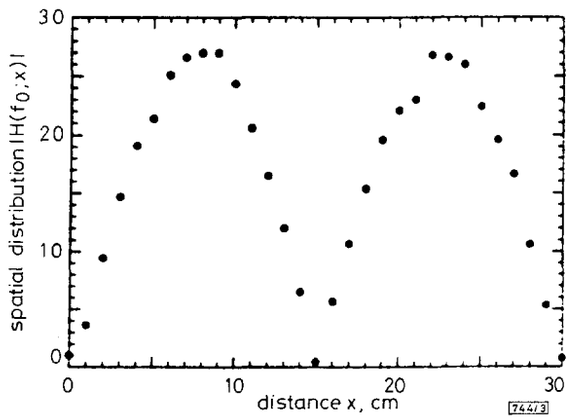

Fig. 3 *Spatial distribution of magnitude of transfer function, $|H(f_0; x)|$ at $f_0 = 136.25$ Hz, obtained in experiment using a brass beam*

Simulation experiments: The spatial distribution of the bending vibration of a brass beam (length $l = 29.7$cm, diameter $2r = 2$mm) is measured using laser Doppler velocimetry. The beam is pin-ended and actuated at its centre ($x = 15$cm) by a small vibrator driven by white noise $n(t)$. Fig. 3 shows the spatial distribution of the magnitude of the transfer function $H(f_0; x)$ for the frequency $f_0 = 136.25$Hz, which corresponds to the standing wave with the second mode. Since wavelength $\lambda_b(f_0) = 0.297$m, the phase velocity $c_b(f_0)$ at $f_0 = 40.5$m/s, by which c_l is determined as being 3826m/s from eqn. 3.

In vivo measurements: The proposed method is applied to the radius ($l = 24$cm) of the left hand of a normal young individual. The vibrator in Fig. 1 is driven by band-limited noise from 80Hz to 4kHz. Fig. 4*a* shows $|H(f_0; x)|$ of eqn. 2 for the frequency component $f_0 = 111$Hz. When the vibration on the skin surface is measured by laser Doppler velocimetry there is no correlation with the driving signal. As shown in Fig. 4*b*, however, the squared

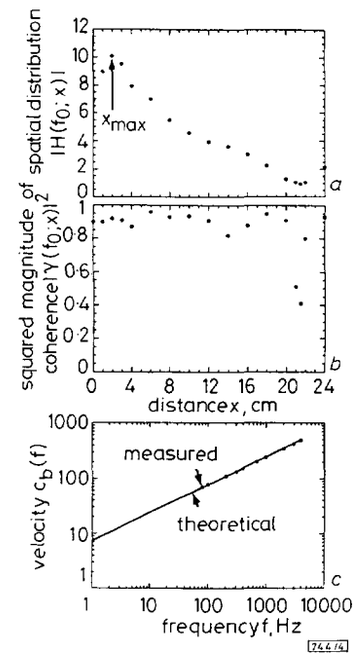

Fig. 4 *In vivo experimental results for radius of a bone in a normal young human subject*

a Spatial distribution of magnitude of transfer function $|H(f_0; x)|$ at $f_0 = 111$Hz
b Squared magnitude of coherence function, $|\gamma(f_0; x)|^2$, between driving white noise $n(t)$ and velocity signal $v(t; x)$ for $f_0 = 111$Hz
c Frequency characteristics of measured velocity $c_b(f)$ of bending vibration

magnitude of the coherence function, $|\gamma(f; x)|^2$, between $n(t)$ and $v(t; x)$ is almost one at points other than the proximal radius, where $|\gamma(f_0; x)|^2$ is defined by

$$|\gamma(f_0;x)|^2 = \frac{|\mathrm{E}[A^*(f_0;x) \cdot B(f_0;x)]|^2}{\mathrm{E}[|A(f_0;x)|^2 \cdot \mathrm{E}[|B(f_0;x)|^2]} \quad (4)$$

Thus, the measurement of the velocity on the bone surface using an ultrasonic probe on the skin surface is effective. From Fig. 4*b*, the wavelength $\lambda_b(f_0)$ is determined as being 0.78m at $f_0 = 111$Hz. Thus, the propagation velocity $c_b(f_0)$ of the radius is 86.6 m/s. Since the spatial distribution is determined by the average operation E[·] in eqn. 2, high accuracy is realised for small vibrations because the velocity at $x_{max} = 2$cm in Fig. 4*a* is 0.084m/s for $f_0 = 111$Hz, which corresponds to a small displacement of 120μm. Fig. 4*d* shows the frequency characteristics of the phase velocity $c_b(f)$ in the frequency range from 80Hz to 4kHz. The measured values are exactly on the straight line of eqn. 3, and from the gradient, c_l is determined to be 2150m/s by assuming that the diameter $2r$ of the radius is uniform at 20mm. The obtained c_l almost coincides with the value of the longitudinal wave of the bone [3].

Conclusions: We have proposed a method for *in vivo* measurement of phase velocity of the bending vibration of a bone to diagnose its mechanical characteristics. This new method is expected to be applied for noninvasive diagnosis of osteoporosis.

4 September 1995
Electronics Letters Online No: 19951350

H. Kanai, M. Park and N. Chubachi (*Department of Electrical Engineering, Faculty of Engineering, Tohoku University, Sendai 980-77, Japan*)

References

1 NOKES, L.D.M., WILLIAMS, J.H., FAIRCLOUGH, J.A., MINTOWT-CZYZ, W.J., and MACKIE, I.G.: 'Literature review of vibrational analysis of human limbs', *IEEE Trans.*, 1984, **BME-31**, (2), pp. 187–192

2 PARK, M., KANAI, H., and CHUBACHI, N.: 'In vivo measurement of bending-vibration propagation-velocity of a bone ultrasonic Doppler method', *J. Acoust. Soc. Jpn.*, 1994, **50**, (2), pp. 103–109 (in Japanese)

3 BRANDENBURGER, G., AVIOLI, L., CHENUT, C., HEANEY, R., POSS, R., PRATT, G., and RECKER, R.: 'In vivo measurement of osteoporotic bone fragility with apparent velocity of ultrasound'. IEEE Ultrasonics Symp., 1989, pp. 1023–1027

Applicability of Walfisch-type urban propagation models

N. Cardona, P. Möller and F. Alonso

Indexing terms: Radiowave propagation, Mobile radio systems

The applicability of different propagation models based on the Walfisch-Bertoni or the Walfisch-Ikegami formulations is studied. When this type of model is applied to real urban cells, large areas with errors often appear. The origin of some errors and a proposal to improve the applicability of Walfisch-type models, based on a measurement campaign, are described.

Over-building propagation: The numerical solution developed by Walfisch [1] yields a value for the settled field against the parameter $v = \alpha\sqrt{d/\lambda}$, where α is the incidence angle and d is the mean building distance. It is assumed that for cellular mobile radio the usual parameters make v range from 0.02 to 0.5, and the $1/R^{0.9}$ dependence is accepted as an approximation for the over-building propagation loss $Q(v)$. This term appears in both models [1, 2]:

Walfisch-Bertoni:

$$18\log R - 18\log\Delta H_{base} - 9\log d + 9\log\lambda$$

Walfisch-Ikegami:

$$18\log R - 18\log(1+\Delta H_{base}) - 9\log d + k_f\log\lambda$$

With a simple analysis the range validity of this approximation can be found. For tlie available digital map (Valencia urban area), mean values for ΔH and d are 20 m and 100m, respectively, and therefore the approximation becomes valid for distances from the transmitter over 730m.

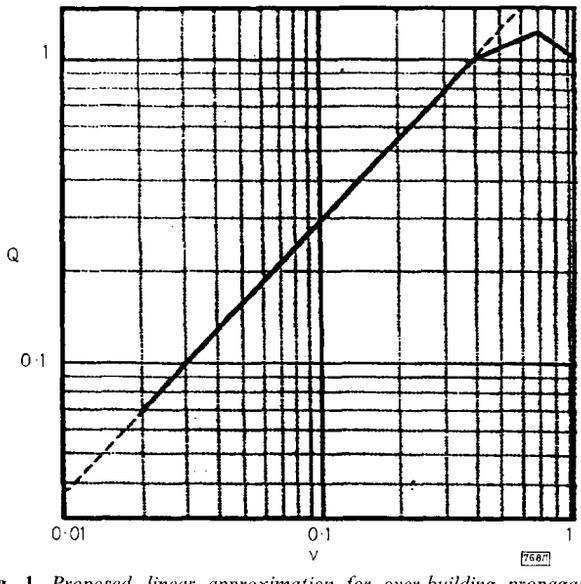

Fig. 1 *Proposed linear approximation for over-building propagation factor Q(v)*

A more detailed study for this urban area showed that a value for $v = 0.5$ is exceeded in more than 60% of the points and the value 1 in more than 25%. The error due to the approximation is > 3dB for $v = 1$ points and > 6dB for $v = 2$ locations. It seems that a more accurate approximation for the over-building propagation term is needed. Two possible solutions are to adopt an explicit theoretical solution [3] or to define a simple linear approximation with four intervals (see Fig. 1):

$$Q(v)_{OBP} \simeq \begin{cases} 2.34v^{0.9} & v < 0.38 \\ 1.40v^{0.37} & 0.38 < v < 0.7 \\ v^{\ 0.57} & 0.7 < v < 1 \\ 1 & 1 < v \end{cases}$$

Using the best fit expression to eliminate the free space and diffraction terms influence, the improvement due to the new linear approximation has been compared with both models:

	Mean(error) dB	Std(error) dB
W – Bertoni	+0.66	6.13
W – Ikegami	+0.67	5.21
Valencia	−0.19	4.75

The assumption of homogeneous regular height for the buildings in the mobile area is not accomplished in general. Measurements in areas with similar characteristics for the final-building diffraction but irregular building heights in the TX-RX plane have been carried out. As a result, it has been proved that for small values of the standard deviation σ_h of the building height the error is not much affected. A range of variations up to two floors can be accepted to fit in with the assumption of regular building heights. If a uniform distribution is assumed, the compensation term is similar to that obtained in [4], i.e.

$$\Delta F = -0.525\Delta h_{roof}$$

where Δh_{roof} is the range of building heights.

Final building diffraction: The final diffraction has been formulated in different ways [1 – 3], but in this study just the Walfisch-type models are considered:

W-Bertoni $L_{FBD} =$

$$-11.8 + 10\log r_2 + 10\log f(\text{MHz}) + 20\log\gamma(\text{rad})\ [\text{dB}]$$

W-Ikegami $L_{FBD} =$

$$-16.9 - 10\log w + 10\log f(\text{MHz}) + 20\log(\Delta h_m)\ [\text{dB}]$$

where w is the street width and r_2 is the distance between the diffraction edge and the receiver.

The parameters used in these models are different but geometrically correlated. In our case the horizontal resolution defining the wall's location is high, but the vertical resolution for the building height is ~±1.5m. This means a range of errors due to vertical resolution of ±1.5dB in the Walfisch-Bertoni model and of ±3dB in the Walfisch-Ikegami model (measured with the Valencia database). Then the Walfisch-Ikegami model is slightly more sensitive to vertical resolution errors.

In the Walfisch-Bertoni model the term

$$F = \frac{\sqrt{\lambda}}{2\pi\sqrt{r_2}}\left(\frac{1}{\beta} - \frac{1}{2\pi+\beta}\right)$$

is approximated by

$$F' \simeq \frac{\sqrt{\lambda}}{2\pi\sqrt{r_2}}\left(\frac{1}{\gamma}\right)$$

where $\gamma = \alpha + \beta$, and it is assumed that α is small compared to γ, and $\beta << 2\pi$, where β is the diffraction angle.

These approximations produce some errors when the model is applied to real urban areas. In an important percentage of points α cannot be neglected in the γ expression. The difference between using the F factor and the approximation F' produces errors in the range of 10dB for small values of β, as is shown in Fig. 2 for the measured locations.

This error is easily corrected by using β instead of γ in the Walfisch-Bertoni factor:

$$L'_{FBD} = -11.8 + 10\log r_2 + 10\log f(\text{MHz}) + 20\log\beta(\text{rad})\ [\text{dB}]$$

Concerning the $\beta << 2\pi$ assumption, the error introduced is not very significant: a maximum error of 1.1dB has been calculated for the measured points.

If the dependencies of the Walfisch-Bertoni model are analysed, it can be seen that for big values of the diffraction angle $\beta >$ 0.5rad) the error is centred around 0dB and more uncorrelated. These are the values of β for which the Walfisch-Bertoni solution is correct, but they correspond to only 40% of the tested points in Valencia. For lower values of β the slope of the error in terms of the diffraction factor is almost 1, which leads to the conclusion